

# Transmission Enhancement Methods for Low-Emissivity Glass at 5G mmWave Band

Hyunjin Kim<sup>✉</sup> and Sangwook Nam<sup>✉</sup>, Member, IEEE

**Abstract**—This letter presents transmission enhancement methods for low-emissivity (low-E) windows at millimeter wavelength (mmWave) frequencies. These methods are required for installation of effective indoor customer premises equipment for mmWave fixed wireless access (FWA) services. Low-pass filtering frequency selective surfaces are patterned with low-E coatings by laser, and the effects are verified theoretically and experimentally. Antireflection (AR) dielectrics are additionally utilized and found to reduce transmission loss in various types of window regardless of frequency and incident angle. The results of the current study achieve lower losses for various types of window and incident angles. A transmission loss improvement is also achieved in a real FWA scenario, which can be applied for the coverage extension of FWA services.

**Index Terms**—5G communication, fixed wireless access (FWA), low-emissivity (low-E) window.

## I. INTRODUCTION

FIXED wireless access (FWA) enables network service providers to deliver ultrahigh-speed broadband to suburban and rural areas, supporting home and business applications where fixed line services are expensive to lay and maintain. In particular, 5G millimeter wavelength (mmWave) FWA [see Fig. 1(a)] can provide a level of bandwidth capacity comparable to fiber optics, and beamformed signals from a 5G AU (access unit) can enable a higher density of users without causing interference. However, the mmWave signal is severely affected by both path and transmission losses [1], [2]. Trees, scattering, and rain attenuation are also obstacles [3]. Outdoor customer premises equipment (CPE) has antenna external to the home or office, and this can mitigate signal degradation. However, indoor CPE is further influenced by high penetration loss through typical building and window materials.

Penetration loss in standard house construction has been worsened recently because of low-emissivity (low-E) glass windows. Low-E glass is used for energy efficiency by minimizing the amount of infrared and ultraviolet light coming through and has a thin transparent coating that reflects heat, as shown in Fig. 1(b). Transmission loss of a double-pane window including a low-E

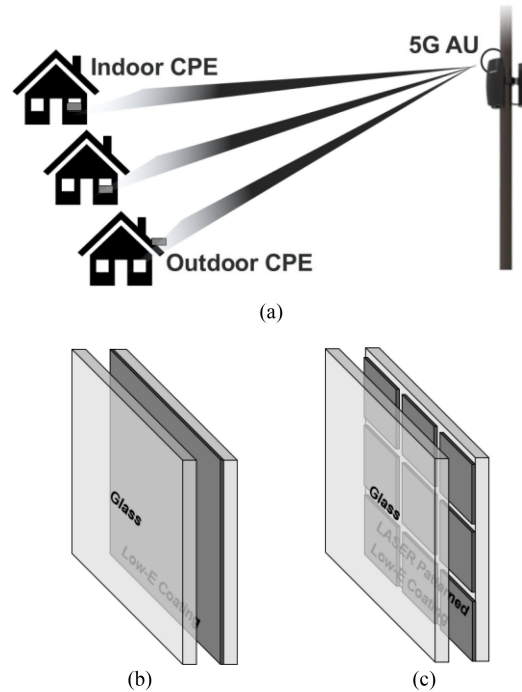


Fig. 1. (a) Commercial 5G FWA configuration. (b) Double-pane window with low-E coating. (c) Double pane-window with patch-patterned low-E coating.

coating has been measured with horn antennas, at below  $-25$  dB [4]. In this letter, a laser-patterned low-E coating is proposed, as illustrated in Fig. 1(c), which is intended to reduce penetration loss while maximizing the energy efficiency of the window [4]–[9]. Using a laser, all kinds of frequency selective surface (FSS) patterns can be applied to the window, including loops, dipoles, patches, and so on [10]. Of these various patterns, a patch array is selected here because of its low-pass filtering characteristic, which can allow mmWave signals while blocking infrared and ultraviolet light. A patch array is also suitable as the etched areas of the low-E coating can be minimized and unnoticeable to the human eyes. Most studies [4]–[9] focus on microwave frequencies from 0 to 3.5 GHz for mobile communications. The most frequently used FSS pattern for the low-E glass is the patch with losses ranging from 0 to 3 dB. One study [9] focuses on a higher frequency range of 26–40 GHz and varying patch size and the gap between the panes, to identify the lowest loss; with a patch size of 0.5 mm, the loss ranged from 3 to 5 dB. The results of the current study achieve lower losses for various types of window and incident angles.

Manuscript received October 23, 2020; revised November 24, 2020; accepted December 1, 2020. Date of publication December 4, 2020; date of current version January 14, 2021. (*Corresponding author: Hyunjin Kim*.)

The authors are with the Samsung Electronics, Suwon 16677, South Korea, and also with the Institute of New Media Communication, School of Electrical and Computer Engineering, Seoul National University, Seoul 08826, South Korea (e-mail: hyunjin7.kim@samsung.com; snam@snu.ac.kr).

Digital Object Identifier 10.1109/LAWP.2020.3042524

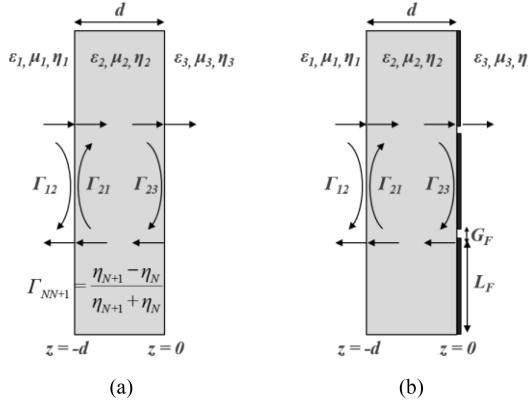


Fig. 2. (a) Reflection coefficients for wave propagation in a single window. (b) Reflection coefficients for a single window with patterned low-E.

## II. REFLECTION COEFFICIENTS OF A SINGLE WINDOW

### A. Theory

In Fig. 2(a), a single lossless window with normal wave incidence is shown, characterized by parameters  $\varepsilon_1, \mu_1$ , and  $\eta_1$ ,  $\varepsilon_2, \mu_2$ , and  $\eta_2$ , and  $\varepsilon_3, \mu_3$ , and  $\eta_3$ . Individual reflection coefficients,  $\Gamma_{NN+1}$ , at each of the boundaries, are also defined, and are referred to as intrinsic reflection coefficients. The input reflection coefficient of a single window [11], [12] can be written as

$$\Gamma_{in}(z = -d) = \frac{\Gamma_{12} + \Gamma_{23}e^{-j2\beta_2 d}}{1 + \Gamma_{12}\Gamma_{23}e^{-j2\beta_2 d}} \quad (1)$$

If on both sides of the window is air,  $\Gamma_{12} = -\Gamma_{23}$ , since  $\eta_1 = \eta_2 = \eta_3$ . The input reflection coefficient is

$$\Gamma_{in}(z = -d) = \frac{\Gamma_{12} - \Gamma_{12}e^{-j2\beta_2 d}}{1 - \Gamma_{12}^2 e^{-j2\beta_2 d}} \quad (2)$$

For the input reflection coefficient to equal zero, the reflection coefficient of (2) must be set to zero. This can be achieved if

$$|\Gamma_{12} - \Gamma_{12}e^{-j2\beta_2 d}| = 0 \quad (3)$$

$$|\Gamma_{12}| |1 - e^{-j2\beta_2 d}| = 0 \Rightarrow 2\beta_2 d = 2n\pi, n = 0, 1, 2 \dots \quad (4)$$

The thickness must be

$$d = \frac{n\pi}{\beta_2} = \frac{n\lambda_2}{2}, n = 0, 1, 2 \dots \quad (5)$$

where  $\lambda_2$  is the wavelength inside the window. The thickness of the window must be an integral number of half-wavelengths inside the dielectric.

A single window with patterned low-E is illustrated in Fig. 2(b). The length of each square patch is  $L_F$  and the gap between patches is  $G_F$ . For the input reflection coefficient to be equal to zero

$$\beta_2 d + \theta_P = n\pi, n = 0, 1, 2 \dots \quad (6)$$

where  $\theta_P$  is the phase difference shifted by the FSS pattern on a window.

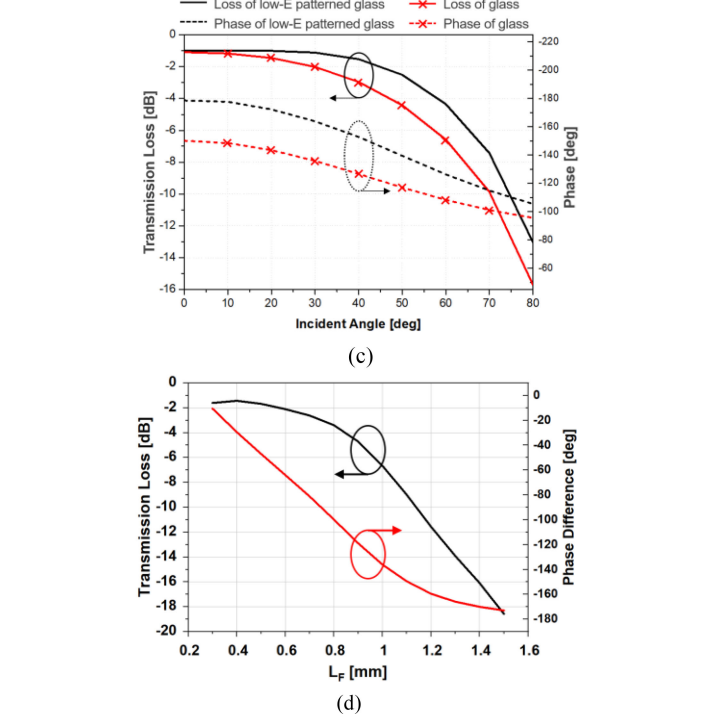
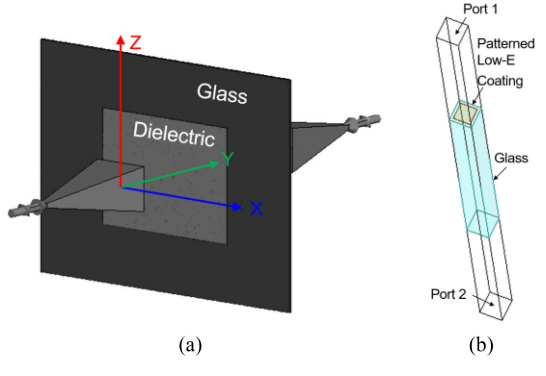


Fig. 3. (a) Simulation models with horn antennas. (b) Simulation model with periodic boundary condition. (c) Simulated transmission loss and phase of a single-pane window with and without low-E pattern. (d) Transmission loss and the phase difference shifted by  $L_F$  of the FSS pattern.

### B. Simulation and Verifications

Fig. 3(a) illustrates a simulation of wideband horn antennas with a single-pane window. Since the permittivity of the glass varies from 3 to 10, the simulated and measured results are compared to find more accurate permittivity and loss tangents. By comparing various results, permittivity is determined to be 6.7 and the loss tangent is 0.009. In Fig. 3(b), the Ansys EM simulation model of a low-E patterned single-pane window is shown. The simulation is performed using periodic boundary conditions extended to an infinite number of elements at each side. Fig. 3(c) plots the simulated transmission loss and phases of single-pane and low-E patterned single-pane windows. The simulation model shown in Fig. 3(b) is used, which compensates the distance from the ports to the glass. The thickness of the glass is 4 mm, and the FSS pattern has  $L_F = 0.3$  mm and  $G_F = 0.025$  mm. The phase of approximately 20° is changed with

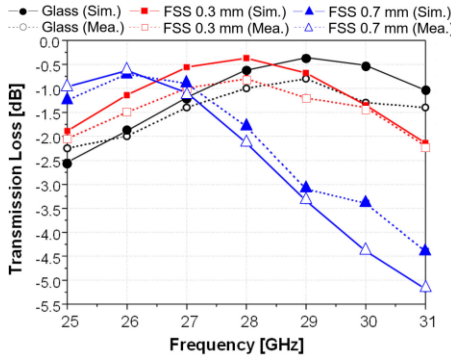


Fig. 4. Compared transmission loss of a single-pane window against frequency.

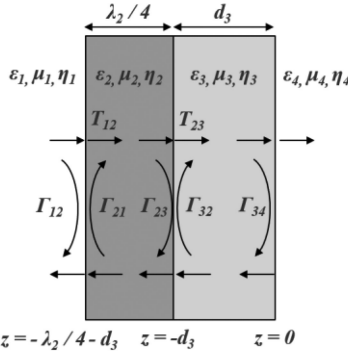


Fig. 5. Single glass with a quarter-wavelength dielectric slab.

the low-E pattern, and the transmission loss is minimized since the phase is near  $n\pi$  for an incident angle of  $0^\circ$ . Moreover, the transmission loss is improved for all incident angles. Fig. 3(d) plots the simulated transmission loss and the phase difference shifted by  $L_F$  of the FSS pattern. While  $G_F$  is fixed, the phase difference and the transmission loss are increased depending on  $L_F$ . Fig. 4 presents the comparison of transmission loss against frequency with the simulation and measurements results in accordance. The measurement is exhibited with two horn antennas and a network analyzer. Transmission loss is minimized at 28 GHz with  $L_F = 0.3$  mm but is lowest with  $L_F = 0.7$  mm at 26 GHz.

### III. REFLECTION COEFFICIENTS OF A DOUBLE WINDOW

#### A. Theory

Since the phase shift generated by a single FSS pattern is limited, an additional dielectric slab is considered for double-pane windows. In Fig. 5, a single window with quarter-wavelength slab is illustrated. From (1), the input reflection coefficient [11]–[13] can be written as

$$\Gamma_{\text{in}}(z = -\lambda_2/4 - d_3) = \frac{\Gamma_{12} - \Gamma_{23}}{1 - \Gamma_{12}\Gamma_{23}}. \quad (7)$$

From the definition of intrinsic reflection

$$\Gamma_{\text{in}}(z = -\lambda_2/4 - d_3) = \frac{\frac{\eta_2 - \eta_1}{\eta_2 + \eta_1} - \frac{\eta_3 - \eta_2}{\eta_3 + \eta_2}}{1 - \frac{\eta_2 - \eta_1}{\eta_2 + \eta_1} \frac{\eta_3 - \eta_2}{\eta_3 + \eta_2}} = \frac{\eta_2^2 - \eta_1\eta_3}{\eta_2^2 + \eta_1\eta_3}. \quad (8)$$

TABLE I  
STANDARD DOUBLE-PANE WINDOWS

	GLASS THICKNESS [MM]	SPACING [MM]	GLASS THICKNESS [MM]
A	3.2	15	3.2
B	3.2	15	4.0
C	3.2	15	4.7
D	4.0	15	4.0
E	4.0	15	4.7
F	4.7	15	4.7
G	6	12	6

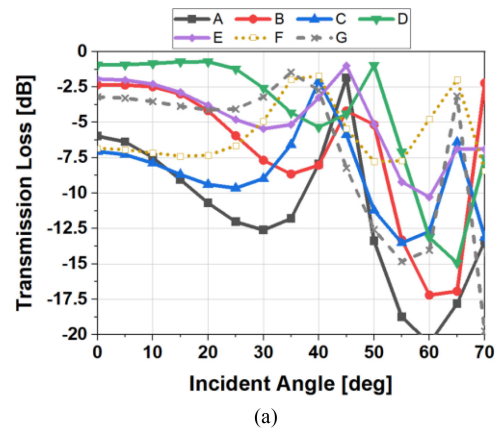


Fig. 6. Transmission loss of various types of double-pane windows. (a) Without and (b) with two dielectric slabs.

If the dielectric slab is made of polycarbonate with permittivity of 2.9 and a loss tangent of 0.012, the reflection coefficient is approximately 0.113. The slab is referred to as an antireflection (AR) dielectric and is also available to double-pane windows.

#### B. Simulation and Verification

Using the periodic boundary simulation condition presented in Fig. 3(b), various patterned low-E double-pane windows are examined. Table I presents commonly used thicknesses and spacing in double-pane windows. The simulated results with and without dielectric slabs are plotted according to the incident angle shown in Fig. 6(a) and (b). Here, the simulated frequency

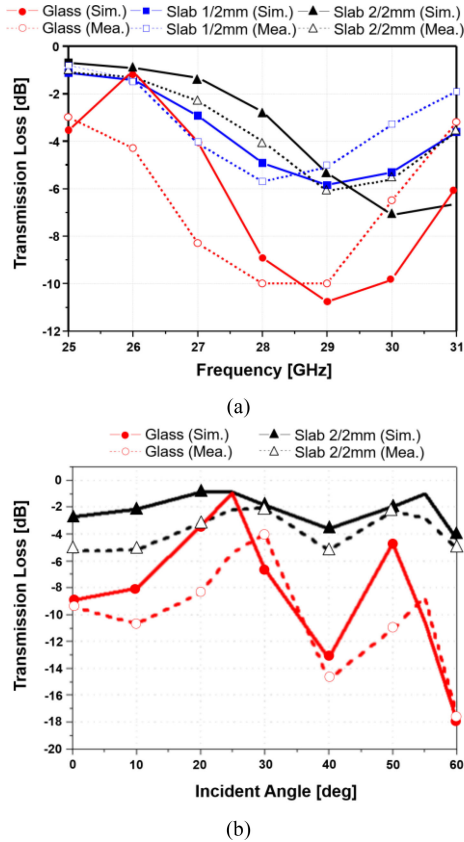


Fig. 7. Transmission loss of double-pane windows with dielectric slabs. (a) Compared results depending on frequency. (b) Compared results depending on the incident angle.

is 28 GHz, and the thickness of the AR dielectric is 1.5 mm, which is around  $\lambda_g/4$  of polycarbonate. Two dielectric slabs are attached on both sides of the window, as the transmission loss is enhanced more and flatter depending on the incident angle. The double-pane windows transmission loss reaches 7.5 dB at an incident angle of 0°, but this can be improved to 2 dB with an AR dielectric. Furthermore, the transmission loss is reduced for all incident angles, and could be further enhanced if the thickness of the dielectric slabs are adjusted for the type of window used.

Fig. 7 presents the comparison of transmission loss between simulated and measured results. A double-pane window with an air gap of 18 mm and pane thicknesses of 3 and 5 mm is measured with horn antennas, as shown in Fig. 3(a). The simulated and measured results are matched, although the measured results demonstrate a shift in Fig. 7(a). Two AR dielectrics of 1 and 2 mm are used for measurement, and the transmission loss is better than that without the slabs for every frequency. The transmission loss is also reduced for all incident angles, as plotted in Fig. 7(b). The loss is lowered by about 6 dB for boresight and 10 dB for a maximally tilted angle.

### C. Practical Results

A prototype window is installed, as shown in Fig. 8(a), to allow practical measurement of a real FWA scenario. A double-pane window with a 3 mm–16 mm–3 mm setup and

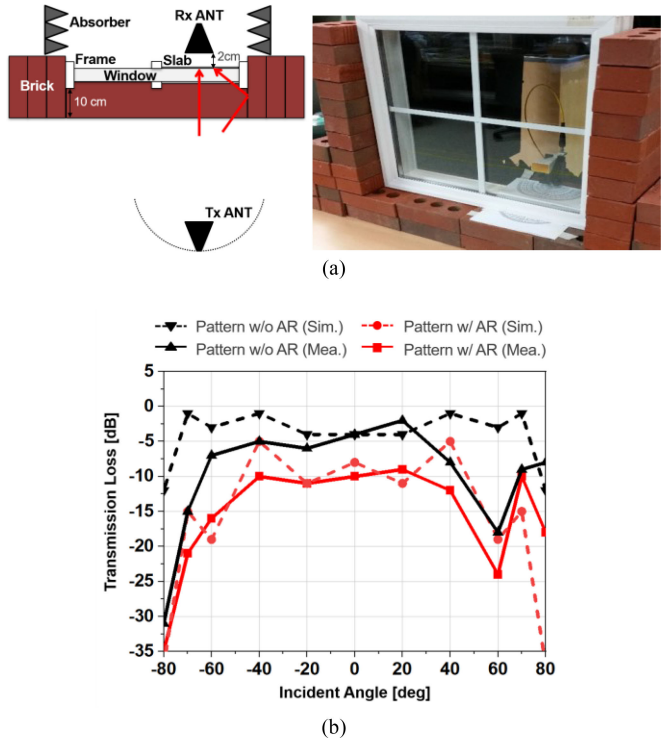


Fig. 8. (a) Indoor CPE environmental setup. (b) Measured results.

laser-patterned low-E glass is used. Two transparent AR dielectrics each with a thickness of 1.5 mm are attached. A receiving horn antenna is positioned 2 cm in front of the window and the transmitting antenna is placed 3 m away. The measurement is also exhibited with a network analyzer. The two antennas are rotated with 20° increments during measurement, and the lowest transmission loss is plotted in Fig. 8(b). The AR slabs enhance the transmission loss regardless of the incident angle by around 5 dB for about 60° coverage of the CPE. However, the measured results are lower than those of the simulated results, particularly for tilted incident angles. These results are because of bricks and frames that reflect and diffract the signals.

## IV. CONCLUSION

Transmission enhancement methods for low-E windows at mmWave frequencies in FWA services have been presented. The effects of the FSS patterns are verified both theoretically and experimentally. AR dielectric slabs are also utilized to further reduce the transmission loss. A transmission loss improvement is achieved in a real FWA scenario, which can be applied for the coverage extension of FWA services.

## REFERENCES

- [1] S. Salous *et al.*, “Radio propagation measurements and modelling for standardisation of the site general path loss model in ITU recommendations for 5G wireless networks,” *Radio Sci.*, vol. 55, Jan. 2020, Art. no. e2019RS006924.

- [2] T. S. Rappaport, Y. Xing, G. R. MacCartney, A. F. Molisch, E. Mellios, and J. Zhang, "Overview of millimeter-wave communications for fifth-generation (5G) wireless networks—With a focus on propagation models," *IEEE Trans. Antennas Propag.*, vol. 65, no. 12, pp. 6213–6230, Dec. 2017.
- [3] J. Huang, Y. Cao, X. Raimundo, A. Cheema, and S. Salous, "Rain statistics investigation and rain attenuation modeling for millimeter wave short-range fixed links," *IEEE Access*, vol. 7, pp. 156110–156120, 2019.
- [4] L. Burnier *et al.*, "Energy saving glazing with a wide band-pass FSS allowing mobile communication: Up-scaling and characterization," *Microw., Antennas Propag.*, vol. 11, no. 10, pp. 1449–1455, Aug. 2017.
- [5] G. I. Kiani *et al.*, "Transmission of infrared and visible wavelengths through energy-saving glass due to etching of frequency-selective surfaces," *Microw., Antennas Propag.*, vol. 4, no. 7, pp. 955–961, Jul. 2010.
- [6] G. I. Kiani, L. G. Olsson, A. Karlsson, K. P. Esselle, and M. Nilsson, "Cross-dipole bandpass frequency selective surface for energy-saving glass used in buildings," *IEEE Trans. Antennas Propag.*, vol. 59, no. 2, pp. 520–525, Feb. 2011.
- [7] L. Liu *et al.*, "Achieving low-emissivity materials with high transmission for broadband radio-frequency signals," *Sci. Rep.*, vol. 7, no. 1, Jul. 2017, Art. no. 4840.
- [8] J. Fleury *et al.*, "Novel microwave transparent low emissivity coating for energy-efficient glazing: Towards 5G frequencies," *J. Phys. Conf. Ser.*, vol. 1343, no. 1, Nov. 2019, Art. no. 012199.
- [9] J. Fleury *et al.*, "Wide band-pass FSS with reduced periodicity for energy efficient windows at higher frequencies," *Appl. Phys., A*, vol. 126, pp. 417, May 2020, Art. no. 417.
- [10] B. A. Munk, *Freq. Selective Surfaces: Theory Des.*. Hoboken, NJ, USA: Wiley, 2000.
- [11] C. A. Balanis, *Advanced Engineering Electromagnetics*. Hoboken, NJ, USA: Wiley, 2012.
- [12] S. J. Orfanidis, *Electromagnetic Waves and Antennas*, 2016. [Online]. Available: [www.ece.rutgers.edu/~orfanidi/ewa](http://www.ece.rutgers.edu/~orfanidi/ewa)
- [13] J. Kim, S. Song, H. Shin, and Y. Park, "Radiation from a millimeter-wave rectangular waveguide slot array antenna enclosed by a Von Karman radome," *J. Electromagn. Eng. Sci.*, vol. 18, no. 3, pp. 154–159, Jul. 2018.